1521-0111/103/6/299–310$35.00
MOLECULAR PHARMACOLOGY

dx.doi.org/10.1124/molpharm.122.000601
Mol Pharmacol 103:299–310, June 2023

Determinants of Subtype-Selectivity of the Anthelmintic Paraherquamide A on *Caenorhabditis elegans* Nicotinic Acetylcholine Receptors[S]

Wataru Koizumi,* Shuya Otsubo,* Shogo Furutani,* Kunihiro Niki,* Koichi Takayama, Shota Fujimura, Takanobu Maekawa, Ryosuke Koyari, Makoto Ihara, Kenji Kai, Hideo Hayashi, Mohammad Shaokat Ali, Eriko Kage-Nakadai, David B. Sattelle, and Kazuhiko Matsuda

Department of Applied Biological Chemistry, Faculty of Agriculture (W.K., S.O., S.Fur., K.N., K.T., S.Fuj., T.M., R.K., M.I., K.M.) and Agricultural Technology and Innovation Research Institute (K.M.), Kindai University, Nara, Japan; Graduate School of Agriculture (K.K., H.H.) and Graduate School of Human Life and Ecology (M.S.A., E.K-N.), Osaka Metropolitan University, Osaka, Japan; Faculty of Food Science and Technology, Chattogram Veterinary and Animal Sciences University, Chattogram, Bangladesh (M.S.A.); and Centre for Respiratory Biology, UCL Respiratory, Division of Medicine, University College London, London, UK (D.B.S.)

Received July 29, 2022; accepted January 27, 2023

ABSTRACT

The anthelmintic paraherquamide A acts selectively on the nematode L-type nicotinic acetylcholine receptors (nAChRs), but the mechanism of its selectivity is unknown. This study targeted the basis of paraherquamide A selectivity by determining an X-ray crystal structure of the acetylcholine binding protein (AChBP), a surrogate nAChR ligand-binding domain, complexed with the compound and by measuring its actions on wild-type and mutant *Caenorhabditis elegans* nematodes and functionally expressed *C. elegans* nAChRs. Paraherquamide A showed a higher efficacy for the levamisole-sensitive [L-type (UNC-38/UNC-29/UNC-63/LEV-1/LEV-8)] nAChR than the nicotine-sensitive [N-type (ACR-16)] nAChR, a result consistent with in vivo studies on wild-type worms and worms with mutations in subunits of these two classes of receptors. The X-ray crystal structure of the *Ls*-AChBP-paraherquamide A complex and site-directed amino acid mutation studies showed for the first time that loop C, loop E, and loop F of the orthosteric receptor binding site play critical roles in the observed L-type nAChR selective actions of paraherquamide A.

SIGNIFICANCE STATEMENT

Paraherquamide A, an oxindole alkaloid, has been shown to act selectively on the L-type over N-type nAChRs in nematodes, but the mechanism of selectivity is unknown. We have co-crystallized paraherquamide A with the acetylcholine binding protein, a surrogate of nAChRs, and found that structural features of loop C, loop E, and loop F contribute to the L-type nAChR selectivity of the alkaloid. The results create a new platform for the design of anthelmintic drugs targeting cholinergic neurotransmission in parasitic nematodes.

Introduction

Paraherquamide A (Fig. 1A) is a polycyclic oxindole alkaloid, first isolated as a toxic metabolite from *Penicillium paraherquei* (Yamazaki et al., 1981). Its anthelmintic activity was demonstrated using gerbils (*Meriones unguiculatus*) infected with a parasitic nematode *Trichostrongylus colubriformi* (Ostlind et al., 1990) and in studies on the nematode genetic model organism *Caenorhabditis elegans* (Ondeyka et al., 1990). Subsequently, paraherquamide A and related compounds were tested on a variety of parasitic nematodes, thereby establishing their broad-spectrum anthelmintic activity (Lee et al., 2002).

Paraherquamide A induced rapid flaccid paralysis in the parasitic nematode *Haemonchus contortus* without affecting ATP concentration, indicating a possible action on nervous system or neuromuscular receptors (Thompson et al., 1996). In the case of *Ascaris suum*, 2-deoxy-paraherquamide A (derquantel) showed a higher paralytic activity than paraherquamide A and thus the mechanism of action of the deoxy-derivative was further examined using an in vitro assay. It reduced ACh-induced contraction of an *A. suum* muscle strip in a manner similar to that seen with mecamylamine and methyllycaconitine, pointing to an action on cholinergic neuromuscular transmission (Zinser et al., 2002). Robertson et al. (2002) tested both paraherquamide A and derquantel for their capacity to block agonist-induced contraction of *A. suum* muscle.

K.M. and M.I. were supported by Grant-in-Aid for Scientific Research (KAKENHI) from the Japan Society for the Promotion of Science [Grant 21H04718 (K.M.); 22H02350 (M.I.)]. D.B.S. was supported by an MRC Programme grant [Grant MR/N024842/1] on which he is co-principal investigator.

No author has an actual or perceived conflict of interest with the contents of this article.

*These authors contributed equally to this study.

dx.doi.org/10.1124/molpharm.122.000601.

[S] This article has supplemental material available at molpharm.aspetjournals.org.

ABBREVIATIONS: ACh, acetylcholine; AChBP, acetylcholine binding protein; CI, confidence interval; nAChR, nicotinic acetylcholine receptor; SOS, standard oocyte saline; SOS-A, SOS containing 0.5 μM atropine.

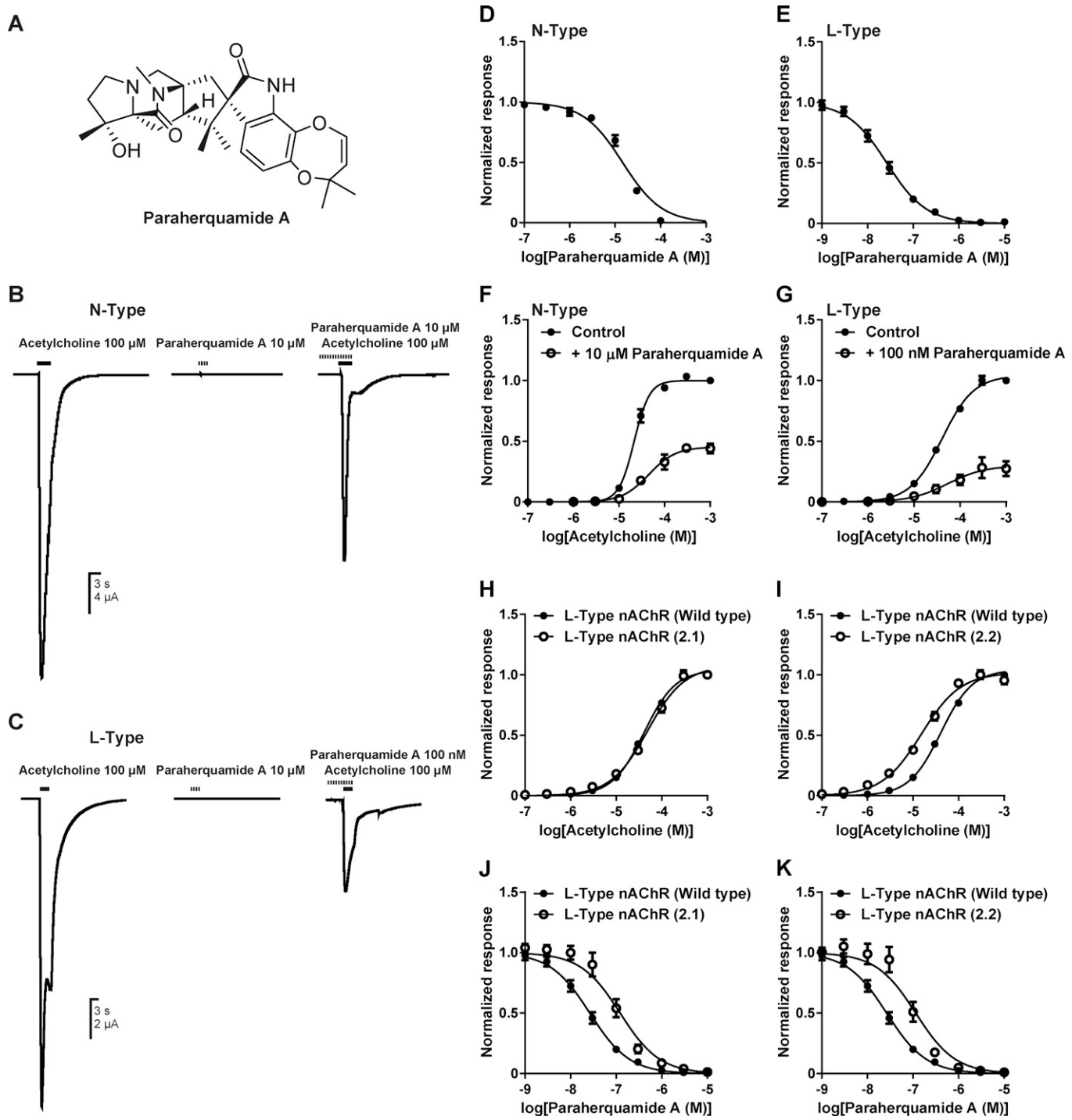

Fig. 1. Paraherquamide A and its effects on *C. elegans* N-type and L-type nicotinic acetylcholine receptors (nAChRs) expressed in *X. laevis* oocytes. Paraherquamide A (A) was bath-applied at 10 μM and 100 nM to oocytes expressing the N-type (B) and L-type (C) nAChR, respectively, for 1 min and then co-applied with 100 μM ACh (B, C). Paraherquamide A reduced the ACh-response of N-type and L-type nAChRs (n = 5). (D, E) Concentration-inhibitory action relationships for paraherquamide A on the N-type (D) and L-type (E) nAChRs. (F, G) Effects of paraherquamide A on the concentration-agonist action relationships for ACh on the N-type (F) and L-type (G) nAChRs. (H–K) Concentration-agonist action relationships of ACh (H, I) and concentration-inhibitory antagonist actions of paraherquamide A (J, K) on *C. elegans* 2.1 and 2.2 L-type nAChRs. Efach data plot represents the mean ± S.E.M. (n = 5).

Both compounds induced parallel shifts to the right of the ACh concentration-response curve, i.e., increased the EC_{50} values, indicating a competitive type of antagonism at nematode nAChRs (Robertson et al., 2002). The nicotine-sensitive (N-type), levamisole-sensitive (L-type), and bephenium-sensitive (B-type) nAChRs expressed on *A. suum* body wall muscles were characterized and the blocking action of paraherquamide A and derquantel were investigated (Robertson et al., 1999). These studies confirmed that paraherquamide A blocked L-type receptors more effectively than N-type receptors in *A. suum*, whereas derquantel was most effective in blocking the B-type receptors, albeit with lower potency than paraherquamide A.

C. elegans is a genetic model organism with a fully sequenced genome and a comprehensive genetic toolkit (*C. elegans* Sequencing Consortium, 1998). The complete *C. elegans* nAChR subunit gene family has been identified (Jones et al., 2007), and the N-type (Ballivet et al., 1996; Raymond et al., 2000; Boulin et al., 2008) and L-type nAChRs (Boulin et al., 2008) have been expressed successfully in *Xenopus laevis* oocytes. A *C. elegans* receptor pharmacologically similar to the native L-type nAChR of *A. suum* results from the co-expression of 8 genes (5x nAChR subunits UNC-38, UNC-29, UNC-63, LEV-1, and LEV-8 co-expressed with 3x auxiliary proteins, RIC-3, UNC-50, and UNC-74), while a *C. elegans* equivalent of the *A. suum* N-type nAChR is obtained by co-expressing the nAChR ACR-16 with the expression-enhancing cofactor RIC-3 (Boulin et al., 2008; Bennett et al., 2012). Using recombinant nAChRs expressed functionally with the aid of auxiliary proteins, the actions of agonists levamisole, pyrantel, and tribendimidine as well as the antagonist derquantel have been described for nAChRs from the important porcine nematode parasite *Oesophagostomum dentatum* (Buxton et al., 2014). Changes in both EC_{50} and maximum nAChR response were observed by adding UNC-38 and LEV-8 to the UNC-63/UNC-29 nAChR. The *C. elegans* L-type 2.1 (UNC-38/UNC-29/UNC-63/LEV-1/ACR-8) and 2.2 (UNC-38/UNC-29/UNC-63/ACR-8) nAChRs were employed to show that the ACR-8 subunit has the capacity to substitute for LEV-8 in the L-type nAChR when expressed in *X. laevis* oocytes (Blanchard et al., 2018). Binding of [^{3}H]paraherquamide A to *C. elegans* membranes was displaced by phenothiazines, members of a previous generation of anthelmintics, suggesting the possibility of a similar site of action (Schaeffer et al., 1992). Omitting ACR-8 from UNC-38/UNC-29/UNC-63/ACR-8 nAChRs was shown to change the action of derquantel from competitive to noncompetitive (Buxton et al., 2014). However, the molecular mechanism underpinning the higher efficacy of these ligands for the L-type than the N-type nAChR remains unknown.

Here we have investigated the mechanism of actions of paraherquamide A on the *C. elegans* N-type (ACR-16) and L-type (UNC-38/UNC-29/UNC-63/LEV-1/LEV-8) nAChRs expressed in *X. laevis* oocytes to address its subtype selectivity and to examine whether it shows competitive or non-competitive actions on *C. elegans* nAChRs. Also, we co-crystallized paraherquamide A with the acetylcholine binding protein from *Lymnaea stagnalis* (*Ls*-AChBP) to elucidate how the ligand-binding, orthosteric site interacts with the compound. We found that paraherquamide A is a much more potent antagonist of the L-type compared with the N-type *C. elegans* nAChR and explored structural features of the nematode nAChR subunits contributing to the L-type nAChR selectivity of the compound.

Materials and Methods

Chemicals

Paraherquamide A was purified *de novo* from the fermentation products of *Penicillium sp.* OK188 strain as follows. The *Penicillium* culture was inoculated with 8 kg of the okara medium and incubated at 25°C for 1 week. The fermentation products were soaked in methanol for 1 week. The methanol extract was partly concentrated and partitioned with an equal volume of ethyl acetate. The ethyl acetate layer was evaporated to yield 34.2 g of residue. The residue was dissolved in a minimal amount of methanol, and water (0.1 volume of methanol) was added to the methanol solution. The aqueous methanol solution was partitioned with hexane (equal volume of the aqueous methanol solution). Methanol was removed from the aqueous methanol layer by evaporation. The remaining aqueous solution was partitioned with ethyl acetate (equal volume of the aqueous solution), and the ethyl acetate layer was evaporated to dryness. The residue (5.06 g) was purified using silica gel column chromatography (Wakogel C-200, Wako Pure Chemical Industries, Japan) with ethyl acetate-methanol mixture [stepwise increase of methanol concentration (5%, 10%, 20%, and 50%)]. Fractions eluted by ethyl acetate containing methanol 0%, 5%, and 10% were collected and evaporated to yield 2.49 g residue, which was purified by silica gel column chromatography using a hexane–acetone mixture with stepwise increase of the acetone concentration (0%, 10%, 20%, 30%, 40%, 50%, 60%, 70%, 80%, 90%, 100%). Fractions eluted with hexane containing 50% and 60% acetone were evaporated to obtain an 800 mg residue, which was further purified by silica gel column chromatography using a chloroform–methanol mixture with stepwise increase of methanol concentration (0%, 0.1%, 0.2%, 0.3%, 0.4%, 0.5%, 0.6%, 0.7%, 0.8%, 0.9%, 1%, 2%, 5%, 10%). Fractions eluted with chloroform containing 0.2%, 0.3%, 0.4%, and 0.5% methanol were collected, and the solvents were evaporated. The resultant solid was recrystallized in ethanol (yield, 157.6 mg), and this recrystallized material was dissolved in methanol to further purify by a preparative HPLC (VP-10 series, Shimadzu, Japan) using a Unison US-C18 column (20 × l50 mm, Imtakt, Japan) with methanol—water mixture (4:1) at a flow rate of 7.5 mL min^{-1} (yield, 25. 3 mg; purity was confirmed to be > 99% by HPLC; Supplemental Fig. 1).

Spectral Data of Paraherquamide A

Specific rotation ($[\alpha]_D^{25}$) of paraherquamide A was determined using a SEPA-300 polarimeter (Horiba, Japan) to be = −17.3 (c = 0.2 dL^{-1}, methanol). Electrospray ionization–mass of the compound was measured using a Q-Tof Premier (Waters, USA) with a 2-propanol/50 mM aqueous NaOH solution containing 0.5% formic acid = 9/1). The observed mass of the protonated molecular ion was 494.2660 (calculated to be 494.2665 for $C_{28}H_{36}O_5N_3$). The ^{1}H- and ^{13}C-NMR spectra were measured in $CDCl_3$ using an Avance System, UltraShield 400 Plus (Bruker BioSpin, USA) (Supplemental Figs. 2 and 3). Chemical shifts δ (ppm) [splitting patterns and coupling constants (Hz)] of the ^{1}H-NMR spectrum (Supplemental Fig. 2) were 0.83 (3H, s, H-23), 1.07 (3H, s, H-22), 1.41 (3H, s, H-28), 1.42 (3H, s, H-27), 1.62 (3H, s, H-17), 1.73∼1.91 (4H, m, H-10b, H-15a, H-19a, H-19b), 2.23 (1H, ddd, J = 4.7, 9.1, 10.8 Hz, H-16b), 2.35 (1H, ddd, J= 4.5, 10.8, 13.3 Hz, H-15b), 2.55 (1H, dd, J= 1.4, 11.2 Hz, H-12b), 2.63 (1H, br s, 14-OH), 2.68 (1H, d, J= 15.3 Hz, H-10a), 3.00 (1H, dd, J=1.5, 11.1 Hz, H-20), 3.03 (3H, s, H-29), 3.21 (1H, ddd, J= 4.5, 9.0, 9.1 Hz, H-16a), 3.60 (1H, d, J=11.2, H-12a), 4.87 (1H, d, J=7.7 Hz, H-25), 6.30 (1H, d, J=7.6 Hz, H-24), 6.67 (1H, d, J=8.0 Hz, H-5), 6.79 (1H, d, J=8.1 Hz, H-4), 7.62 (1H, s, H-N1). Chemical shifts δ (ppm) of the ^{13}C-NMR spectrum (Supplemental Fig. 3) were 19.1 (C-17), 20.4 (C-22), 22.0 (C-19), 23.6 (C-23), 25.9 (C-29), 29.7 (C-28), 29.9 (C-27), 37.0 (C-10), 38.0 (C-15), 46.3 (C-21), 51.4 (C-20), 51.8 (C-16), 59.0 (C-12), 63.0 (C-3), 65.2 (C-11), 71.3 (C-13), 78.0 (C-14), 79.7 (C-26), 115.0 (C-25), 117.2 (C-5), 120.3 (C-4), 124.9 (C-9), 132.4 (C-8), 135.2 (C-7), 138.9 (C-24), 146.0 (C-6), 171.3 (C-18), 182.6 (C-2). These NMR spectral data were in agreement with those reported previously (Blanchflower et al., 1991).

ACh chloride, levamisole, and (-)-nicotine were purchased from MilliporeSigma (USA). Derquantel was purchased from Santa Cruz Biotechnology (USA). These compounds were >95% pure.

cRNA Preparation

The cRNAs encoding the *C. elegans* nAChR subunits and auxiliary proteins RIC-3, UNC-50 and UNC-74 were prepared using the mMESSAGE mMACHINE T7 ULTRA kit (Thermo Fisher Scientific, USA) from their cDNAs (Accession number: ACR-16, AY523511.1; UNC-38, X98600.1; UNC-29, NM_059998.4; UNC-63, AF288374.1; LEV-1, X98601.1; LEV-8, NM_077531.4; ACR-8, NM_001375112; RIC-3,

NM_068898.4; UNC-50, NM_066878.3; UNC-74, accession number not determined). The cDNAs encoding the L-type nAChR subunits UNC-38, UNC-29, UNC-63, LEV-1, LEV-8, as well as those encoding the auxiliary proteins RIC-3, UNC-50, and UNC-74 were gifts from Prof. Thomas Boulin. The cRNAs were dissolved in RNase-free water and mixed at a final concentration of 50 ng μL^{-1} of each subunit and auxiliary protein. Then 50 nL of this RNA mixture solution was injected into *X. laevis* oocytes. When measuring the effects of (-)-nicotine and levamisole on the YPSCC mutant of the N-type nAChR, the RNA concentration was 500 ng μL^{-1} to confirm that they had no agonist action on this nAChR (see later discussion of the results).

Expression of *C. elegans* nAChRs in *Xenopus laevis* Oocytes

An ethical statement for experiments using the frogs is not required in Japan but, as a UK scientist was involved, all our experiments followed the standards of the UK legislation. Oocytes (stage V or VI) were excised from female *X. laevis* anesthetized by benzocaine according to the UK Animals (Scientific Procedures) Act, 1986. We also minimized the use of frogs as much as possible. After treating the excised oocytes for 15 min with 2.0 mg mL^{-1} collagenase (Type IA, MilliporeSigma) in Ca^{2+}-free standard oocyte saline (SOS) containing100 mM NaCl, 2 mM KCl, 1 mM $MgCl_2$, and 5 mM HEPES 5.0 (pH 7.6), they were moved into SOS consisting of 100 mM NaCl, 2 mM KCl, 1.8 mM $CaCl_2$, 1 mM $MgCl_2$, and 5 mM HEPES 5.0 (pH 7.6). The follicle cell layer was removed and the cytoplasm of defolliculated oocytes was injected with 50 nL of the cRNA solution mix encoding either the N-type nAChR (ACR-16 with accessory protein RIC-3) or the L-type nAChR (UNC-38, UNC-29, UNC-63, LEV-1, LEV-8 with the accessory proteins RIC-3, UNC-74, and UNC-50) and incubated at 18°C in SOS supplemented with penicillin (100 units mL^{-1}), streptomycin (100 μg mL^{-1}), gentamycin (50 μg mL^{-1}), 2.5 mM sodium pyruvate, and 4% horse serum (Thermo Fisher Scientific, #26050–070) for 2 to 5 days prior to electrophysiological experiments.

Voltage-Clamp Electrophysiology

The ACh-induced nAChR responses were recorded in SOS containing 0.5 μM atropine (SOS-A), which was added to suppress any possible endogenous muscarinic responses, at 18–23°C (Matsuda et al., 1998). Oocytes were secured in a recording chamber and perfused with SOS-A at a flow rate of 7 to 10 mL min^{-1}. Membrane currents were recorded at a holding potential of −100 mV. The electrodes were filled with 2 M KCl and had a resistance of 0.3 to 5 MΩ in SOS-A. Signals were digitized at a frequency of 1 kHz, recorded, and analyzed using with pCLAMP software (Molecular Devices, USA). ACh was dissolved in SOS-A, while paraherquamide A was dissolved in dimethyl sulfoxide at 10 mM and then diluted with SOS-A immediately prior to experiments. DMSO concentrations in test solutions were 0.1% or lower, at which the solvent had no effect on the nAChR response to ACh and the actions of paraherquamide A. ACh was applied to oocytes for 3 to 5 s, with an interval of 3 min between applications. When testing the blocking action of paraherquamide, ACh was first applied several times until the oocyte response amplitude became stable. Then paraherquamide A was applied for 1 min prior to co-applications with ACh.

Analysis of Current Data

The amplitude of the ACh-induced current was normalized to that of the response at which it reached a plateau (I_{max}). The ACh concentration–response curves in the presence and absence of paraherquamide A and the paraherquamide A concentration-inhibition curves were fitted with Eq. (1) and (2), respectively, using Prism 9 (GraphPad Software, USA):

$$Y = \frac{I_{max}}{1 + 10^{(\log EC_{50} - [L])n_H}} \quad (1)$$

$$Y = \frac{1}{1 + 10^{([L] - \log IC_{50})}} \quad (2)$$

where Y is the normalized response, I_{max} is the normalized maximum ACh response, EC_{50} (M) is the half maximal effective concentration, IC_{50} (M) is the half inhibition concentration (M), [L] is the logarithm of the concentration of ligand (M), and n_H is the Hill coefficient.

Toxicity of Paraherquamide A on *C. elegans*

C. elegans [Strains N2 (wild-type), RB918 *acr-16* (*ok789*) V (N-type nAChR mutant), ZZ20 *unc-38* (*x20*) I (L-type nAChR mutant), ZZ37 *unc-63* (*x37*) I (L-type nAChR mutant)] were obtained from the Caenorhabditis Genetics Center. Effects of the compounds on swimming (thrashing movements) of the worms were investigated as previously reported (Ondeyka et al., 1990). pLC_{50} values (= $-\log LC_{50}$), where LC_{50} is the half lethal concentration (M) for paraherquamide A on the wild-type and mutant worms, were determined by nonlinear regression with Prism 9 according to Eq. (2) in which IC_{50} is replaced by LC_{50}.

Crystallization of *Ls*-AChBP Complexed with Paraherquamide A

The wild-type *Ls*-AChBP was expressed in the yeast *Pichia pastoris* X-33 strain as described previously (Ihara et al., 2014). Secreted proteins were concentrated using a Vivaflow 200 Cross Flow Cassette (Sartorius, Germany) and purified with a Source 30Q column (Cytiva, USA). The *Ls*-AChBP was treated overnight at 37°C with His-tagged endo-*β*-*N*-acetylglycosidase H (Endo H, gene accession number K02182), where Endo H was expressed in *Escherichia coli* BL21 (DE3) and purified by Ni-NTA column chromatography. The protein was further purified with a Mono Q column followed by a Superdex 200 (Cytiva). Purified *Ls*-AChBP was dialyzed over 20 mM Tris-HCl buffer (pH 7.5) and its concentration adjusted to 5.0 mg/mL. The *Ls*-AChBP complexed with paraherquamide A was crystallized by sitting drop vapor diffusion method. Crystals of the complex were flash cooled in liquid nitrogen and stored in liquid nitrogen prior to X-ray diffraction data collection.

X-Ray Crystallography

X-ray diffraction data were collected at 100 K with a RAYONIX MX225HE detector at BL26B1 located at SPring-8, the third-generation synchrotron facility in Harima Science Park City, Hyogo, Japan. Diffraction data were processed using the Aimless (CCP4: supported program) (Winn et al., 2011; Evans and Murshudov, 2013) along with XDS (Kabsch, 2010). The initial phase was obtained by molecular replacement with PHASER (McCoy, 2007) using a protein coordinate: 2ZJU. Refinement of the structure model was performed using Refmac5 (Murshudov et al., 2011), and manual model building was performed with Coot (Emsley and Cowtan, 2004). Two-dimensional figures and cartoon/stick models of the crystal structure of the *Ls*-AChBP-paraherquamide A complex were illustrated by LIGPLOT (Wallace et al., 1995) and PyMoL (Schrödinger, USA), respectively.

Modeling Proteins in Complex with Ligands

Prior to modeling, structure coordinates of paraherquamide A and derquantel were prepared using Chem3D software and AutoDock Tools 1.5.7. Derquantel was docked into *Ls*-AChBP after removing water and paraherquamide A from the X-ray crystal structure of the protein complexed with paraherquamide A. For modeling the ACR-16 protein complexed with paraherquamide A, ACR-16 was aligned with *Ls*-AChBP using MAFFT 7.308 (Katoh et al., 2002; Katoh and Standley, 2013). Then the aligned region corresponding to amino acid number 23 – 228 of *C. elegans* ACR-16 was modeled with MODELER 10.1 using the AutoModel algorithm (Webb and Sali, 2016). Paraherquamide A was docked into the homology model of wild-type ACR-16 using AutoDock Vina 1.1.2 (Trott and Olson, 2010).

Statistical Analysis

Differences of the means were analyzed by parametric methods [*t* test (two-tailed) or one-way ANOVA (Dunnett test)] in which post

hoc tests were conducted only when F values were <0.05. The difference compared was judged significant at $P < 0.05$ level.

Results

Actions of Paraherquamide A on N-type and L-type *C. elegans* nAChRs

First we tested paraherquamide A alone on oocytes expressing either the N-type (ACR-16) or the L-type (UNC-38/UNC-29/UNC-63/LEV-1/LEV-8) *C. elegans* nAChRs. Paraherquamide A had no detectable effect on the membrane currents when applied at 10 μM (Fig. 1, B and C), indicating that it had no detectable agonist action on either receptor at this concentration. Next we perfused nAChR-expressing oocytes with paraherquamide A (N-type, 10 μM; L-type, 100 nM) for 1 min prior to applying ACh at 100 μM. These paraherquamide A exposures reduced the ACh response of N-type and L-type nAChRs by 31.6 [95% confidence interval (CI)]: 14.5–48.8) and 76.4 (95% CI, 68.0–84.8), respectively (Fig. 1, B and C). We evaluated the antagonist potency of paraherquamide A by treating oocytes expressing the N-type nAChR with the alkaloid for 1 minute and then co-applying ACh at 10 μM, which is close to the EC_{50} for ACh (Table 1). Paraherquamide A reduced the peak ACh response of the N-type nACh with a pIC_{50} [= $-\log IC_{50}$ (M)] of 4.84 (95% CI, 4.76 – 4.91) (Fig. 1D; Table 1).

In a similar way, we also treated oocytes expressing the L-type (UNC-38/UNC-29/UNC-63/LEV-1/LEV-8) nAChR with paraherquamide A for 1 minute prior to co-application with 30 μM ACh. Paraherquamide A also reduced the peak current amplitude of the ACh response of the L-type nAChR with a pIC_{50} of 7.58 (95% CI, 7.51 – 7.64) (Fig. 1E; Table 1). The nAChR blocking potency measured as pIC_{50} was higher for the L-type nAChR compared with the N-type nAChR. Derquantel also blocked the ACh-responses of the N-type (ACR-16) and L-type (UNC-38/UNC-29/UNC-63/LEV-1/LEV-8) nAChRs [N-type, pIC_{50} values of 4.76 (95% CI, 4.63 – 4.89)]; L-type 6.03 (95% CI, 5.94 – 6.11) with preference for L-type over N-type nAChRs (Supplemental Fig. 4). Since paraherquamide A was 35.5-fold more potent on the L-type nAChR than derquantel, we focused on the mechanism of selectivity of paraherquamide A to the *C. elegans* L-type over N-type nAChRs.

Prior to investigating the effects of paraherquamide A, we first measured the concentration-response curves for ACh for the N-type (ACR-16) and L-type (UNC-38/UNC-29/UNC-63/LEV-1/LEV-8) nAChRs. ACh activated the N-type nAChR with pEC_{50} (= $-\log EC_{50}$) of 4.67 (95% CI, 4.63 – 4.70) (Fig. 1F; Table 1), whereas it activated the L-type nAChR with pEC_{50} of 4.39 (95% CI, 4.34 – 4.44) (Fig. 1G; Table 1). These data are comparable to those reported previously (Boulin et al., 2008). We then investigated the effects of 10 μM paraherquamide A on the ACh concentration-response curve for the N-type nAChR. The compound shifted the ACh concentration-response curve to the right [pEC_{50} = 4.35 (95% CI, 4.18 – 4.52)], $P < 0.05$, two-tailed t test) and reduced the amplitude of the normalized maximum response [I_{max} = 0.453 (95% CI 0.395 – 0.510), $P < 0.05$, two-tailed t test] (Fig. 1F), suggesting mixed competitive and noncompetitive interactions with the N-type nAChR. On the other hand, 100 nM paraherquamide A reduced the maximum response of the L-type nAChR [I_{max} = 0.300 (95% CI, 0.190 – 0.409), $P < 0.05$, two-tailed t test], while hardly shifting pEC_{50} [4.27 (95% CI, 3.75 – 4.79)] (Fig. 1G), indicating noncompetitive interactions with the L-type nAChR.

To examine the role of the L-type nAChR subunits UNC-38, UNC-29, UNC-63, LEV-1, and LEV-8 in determining paraherquamide A sensitivity, we tested the compound on the L-type 2.1 (UNC-38/UNC-29/UNC-63/LEV-1/ACR-8) and 2.2 (UNC-38/UNC-29/UNC-63/ACR-8) nAChRs. Replacing the LEV-8 subunit by the ACR-8 subunit had a minimal impact on the concentration-response curve for ACh (Fig. 1H). However, omitting the LEV-1 subunit shifted it (Fig. 1I). The 2.1 nAChR showed lower paraherquamide A sensitivity than the L-type (UNC-38/UNC-29/UNC-63/LEV-1/LEV-8) nAChR but > 100-fold higher sensitivity than the N-type (ACR-16) nAChR (Fig. 1J; Table 1). Omitting the LEV-1 subunit from the 2.2 nAChR had a minimal impact on the paraherquamide A sensitivity (Fig. 1K; Table 1).

TABLE 1

Agonist actions of acetylcholine and antagonist actions of paraherquamide A on acetylcholine for the *Caenorhabditis elegans* N-type and L-type nAChRs expressed in *Xenopus laevis* oocytes[a]

	Acetylcholine pEC_{50}	Paraherquamide A[b,c] pIC_{50}
N-Type nAChR		
Wild-type	4.67 (4.63 – 4.70)	4.84 (4.76 – 4.91)
YPSCC (loop C)	4.01 (3.95 – 4.06)*	5.28 (5.20 – 5.36)*
YPCC (loop C)	3.34 (3.30 – 3.37)*	5.54 (5.43 – 5.65)*
V138E (loop E)	3.24 (3.16 – 3.33)*	5.21 (5.11 – 5.31)*
F184V (loop F)	4.72 (4.64 – 4.81)	5.45 (5.30 – 5.59)*
L-Type nAChR		
Wild type	4.39 (4.34 – 4.44)	7.58 (7.51 – 7.64)
YDCC (loop C, UNC-38)	4.37 (4.31 – 4.44)	7.37 (7.28 – 7.46)*
YDCC (loop C, UNC-63)	4.48 (4.42 – 4.53)	7.31 (7.23 – 7.38)*
E142V (loop E, UNC-38)	4.23 (4.17 – 4.30)*	7.15 (7.03 – 7.27)*
V193F (loop F, UNC-29)	4.41 (4.34 – 4.47)	6.87 (6.80 – 6.94)*
V201F (loop F, LEV-1)	4.40 (4.33 – 4.48)	7.05 (6.96 – 7.14)*
2.1	4.31 (4.24 – 4.39)	6.91 (6.79 – 7.03)*
2.2	4.82 (4.74 – 4.90)*	6.94 (6.80 – 7.08)*

*Indicates that difference from the wild-type nAChR is significant ($P < 0.05$, one-way ANOVA, Dunnett test).
[a]Data are shown as the mean (95% CI) (n = 5).
[b]Paraherquamide A was > 95% pure by HPLC analysis (see Supplemental Material).
[c]For wild-type and F184V mutant N-type nAChRs, 10 μM; for YPSCC mutant N-type nAChR,100 μM; for V138E mutant N-type nAChR and YPCC mutant N-type nAChR, 500 μM; for wild-type and mutant L-type nAChRs, 30 μM.

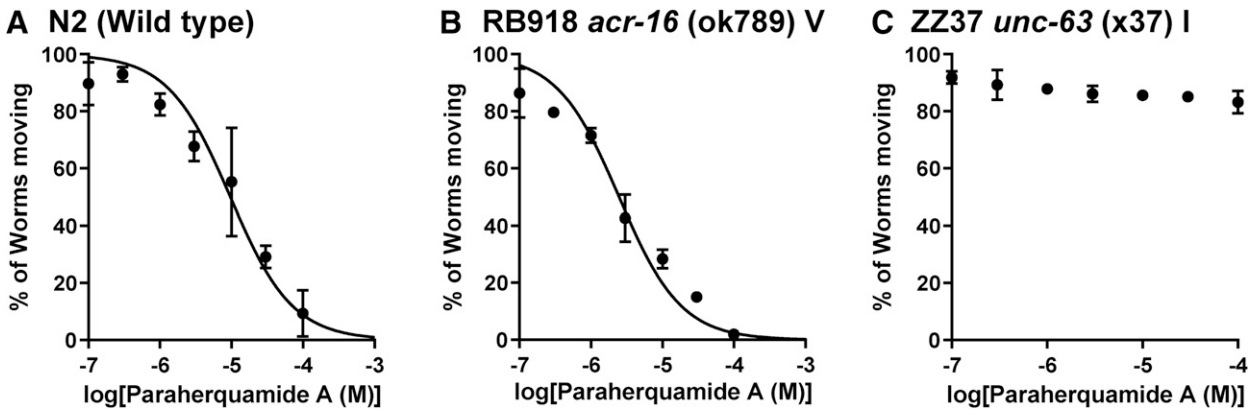

Fig. 2. Actions of paraherquamide A on motility of wild-type and mutant *C. elegans*. (A) Wild-type (N2). (B) Mutant (RB918 *acr-16* (*ok789*) V). (C) Mutant (ZZ37 *unc-63* (*x37*) I). Each data plot represents the mean ± S.E.M. (n = 5).

Actions of Paraherquamide A on Wild-type and Mutant *C. elegans*

We investigated the effects of paraherquamide A on thrashing of wild-type and mutant *C. elegans* to confirm its selectivity for the L-type nACR in vivo. The compound suppressed thrashing of the wild-type worms with pLD_{50} of 5.02 (95% CI, 4.91 – 5.12) (Fig. 2A). Paraherquamide A inhibited thrashing of *C. elegans* with a mutation in the ACR-16 subunit [RB918 *acr-16* (*ok789*) V] with pLC_{50} of 5.61 (95% CI, 5.52 – 5.69) (Fig. 2B), showing higher paraherquamide A sensitivity than the wild-type worms. We failed to determine the activity on the UNC-38 mutant [ZZ20 *unc-38* (*x20*) I] because of its considerably reduced motility even in the absence of the compound, although we could measure activity on worms with a mutation in the *unc-63* gene [ZZ37 *unc-63* (*x37*) I]. The UNC-63 mutant worms were highly resistant to paraherquamide A (Fig. 2C), confirming a preference of the compound for L-type over N-type AChRs.

X-Ray Crystal Structures of *Ls*-AChBP in Complex With Paraherquamide A

The AChBPs have been used to investigate the mechanism of action of various ligands interacting with the orthosteric sites of nAChRs. Having observed the competitive paraherquamide A interactions with ACh at the N-type nAChR (Fig. 1F), we co-crystallized paraherquamide A with the *Ls*-AChBP. When crystallized in 14.1% to 15.6% PEG 4000 in sodium citrate buffer (pH 5.0) at 20°C, the *Ls*-AChBP-paraherquamide A complex resulted in a crystal with a space group of P65 diffracting at a resolution of 2.2 Å (Table 2). We therefore refined its crystal structure with the amino acid sequence shown in Fig. 3A. The electron densities for the ligand were observed at all five interfaces between protomers (Fig. 3B; see Supplemental Fig. 5 for detailed omit maps). Paraherquamide A interacted with the *Ls*-AChBP at ligand binding loops A, B, C, D, E and F (Fig. 3C). The Ser186 and main chain of Cys187 in loop C, as well as the hydroxy group of Tyr164 in loop F formed hydrogen bonds via a water with the carbonyl group in the amide bond of paraherquamide A (Fig. 3, C and D). The mainchain of Trp143 in loop B formed a hydrogen bond with the bridgehead nitrogen of paraherquamide A (Fig. 3C, arrowed). Tyr192 in loop C and the main chain carbonyl of Trp143 in loop B formed hydrogen bonds with the hydroxy group of paraherquamide A (Supplemental Fig. 6). Trp53 (loop D), Tyr89 (loop A), Met114 (loop E), Tyr185 (loop C), and Tyr192 (loop C) made hydrophobic contacts with the compound (Fig. 3, C and E). In loop C, UNC-38, UNC-63, and LEV-8 of the L-type nAChR have a proline, while ACR-16 N-type nAChR subunit has an aspartate (Fig. 3A). In loop E, UNC-38 of the L-type nAChR has Glu142, which corresponds to Met114 in the *Ls*-AChBP (Fig. 3A), and has a negative charge favorable for interactions with a nitrogen of paraherquamide A (Fig. 3, C and E), whereas ACR-16 has Val138 with no negative charge at the corresponding position.

The Effects of Mutations in Loop C and E of N- and L-type nAChRs on the Actions of Paraherquamide A, (-)-Nicotine, and Levamisole

To examine whether loop C interacts with paraherquamide A as in the crystal structure of the *Ls*-AChBP complex, we investigated the effects of replacing its YDCC sequence in loop C of ACR-16 (N-type nAChR) by the YPSCC sequence of UNC-

TABLE 2
X-ray diffraction data for the *Ls*-AChBP-paraherquamide A complex

PDB ID	7DJI
Beamline	SPring-8 BL26B1
Wavelength(Å)	1.0
Space group	P65
Cell dimensions a, c (Å)	74.373, 349.595
Resolution(Å)[a]	47.37–2.20 (2.26–2.20)
Unique reflections[a]	55263 (4552)
R_{merge}[a]	0.710 (0.713)
R_{pim}[a]	0.033 (0.436)
R_{meas}[a]	0.078 (0.841)
$CC_{1/2}$[a]	0.999 (0.0806)
I/σ[a]	21.7 (2.7)
Completeness (%)[a]	100.0 (100.0)
Redundancy[a]	10.8 (7.1)
Refinement	
Resolution(Å)[a]	47.374–2.200 (2.257–2.200)
No. of reflections[a]	55135 (3906)
Completeness (%)[a]	99.94 (99.98)
R/R_{free}(%)[a]	0.185 / 0.231 (0.268/0.295)
RMSD Bond length (Å)/angles(deg)	0.0057 / 0.224
Average B factor for all atoms	49.02
Average B factor for protein atoms	52.55
Average B factor for bound ligands	49.90

[a]Values in parentheses represent those for the highest resolution shell.
RMSD, root mean square deviation.

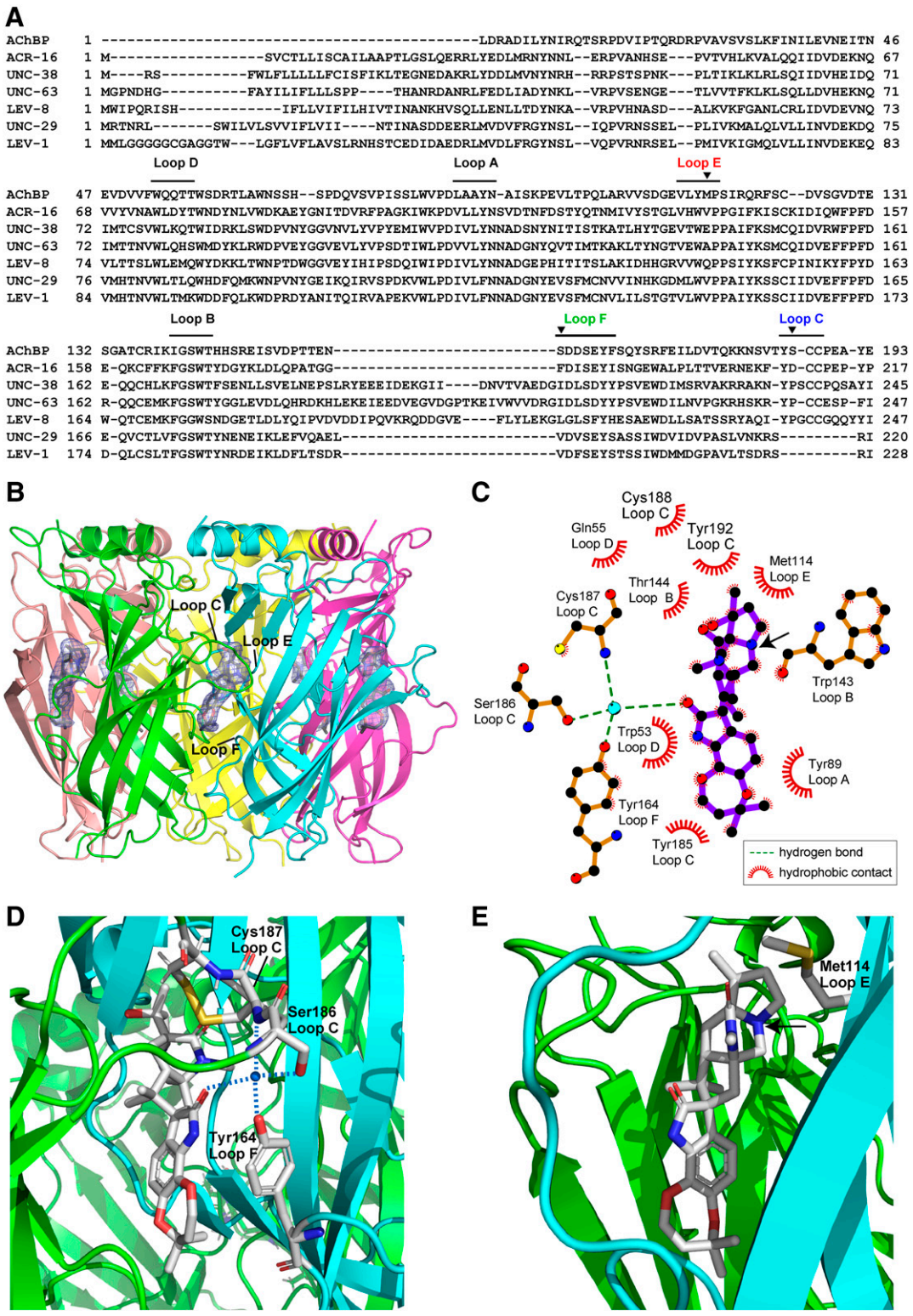

Fig. 3. Crystal structure of *Ls*-AChBP complexed with paraherquamide A. (A) Amino sequences of the N-terminal domain of *C. elegans* nAChR subunits and the *Ls*-AChBP. Positions of amino acids unique to the L-type nAChR subunits are indicated by ▼ (B) Side view of the complex in which paraherquamide A molecules bound at five subunit interfaces. Paraherquamide A is shown with electron density maps (omit map at contour level of root mean square deviation 3.0). (C) LigPlot of paraherquamide A interactions with amino acid residues or main chains in the *Ls*-AChBP. Carbons, nitrogens, oxygens, and sulfur are colored black, blue, red, and yellow, respectively, while water is colored cyan. Tyr89 (loop A), Trp53 (loop D), and Tyr192 (loop C) made hydrophobic contacts. Tyr164 (loop F), Ser186 (loop C), and the main chain nitrogen of Cys187 (loop C) formed hydrogen bonds with a carbonyl oxygen in paraherquamide A. Dashed lines indicate hydrogen bonds. (D, E) Close views of the interactions of the *Ls*-AChBP with paraherquamide A. (D) Hydrogen bonds shown by dashed lines were observed between Tyr164, Ser186, the main chain of Cys187, and one of the carbonyl groups in paraherquamide A via water. (E) Met114 (loop E) located in the vicinity of the bridgehead nitrogen arrowed in paraherquamide A. The principal and complementary chains are colored green and cyan, respectively, while carbons, nitrogens, oxygens, sulfurs, and water are colored gray, blue, red, yellow, and sky blue, respectively. The bridgehead nitrogen is arrowed.

38 (L-type nAChR) on paraherquamide A actions (see Fig. 3A for amino acid sequence comparisons). Switching this loop C segment lowered the pEC_{50} value of ACh to 4.01 (95% CI, 3.95 – 4.06) (Fig. 4A; Table 1). The pIC_{50} of paraherquamide A determined in terms of reduction of the response to 100 μM ACh was increased significantly by the mutation to 5.28 (95% CI, 5.20 – 5.36) (Fig. 4B; Table 1). A reciprocal loop C switch in the UNC-38 of the L-type nAChR, replacing the YPSCC sequence by the YDCC sequence of the N-type (AChR-16) nAChR subunit, had a minimal effect on the agonist potency of ACh (Fig. 4C; Table 1). However, the mutation reduced the antagonist potency of paraherquamide A to 7.37 (95% CI, 7.28 – 7.46) (Fig. 4D; Table 1). Further, loop C of ACR-16 was mutated from YDCC to YPCC, as seen in UNC-63, resulting in enhanced paraherquamide A sensitivity to pIC_{50} of 5.54 (95% CI, 5.43 – 5.65) (Fig. 4B; Table 1). In contrast, replacing the loop C of UNC-63 L-type nAChR subunit from YPCC by YDCC seen in AChR-16 subunit reduced sensitivity [pIC_{50} = 7.31 (95% CI, 7.23 – 7.38), Fig. 4D; Table 1].

As described previously, Met114 in loop E was in the vicinity of the bridgehead nitrogen of paraherquamide A in the crystal structure of the *Ls*-AChBP (Fig. 3E). Since Met114 corresponds to Val138 and Glu142 in the ACR-16 (N-type nAChR) and UNC-38 (L-type nAChR) subunits, respectively (Fig. 3A), Val138 was mutated to glutamate in the ACR-16 subunit. As a result, the antagonist potency in terms of pIC_{50} of paraherquamide A on the N-type nAChR was increased to 5.21 (95% CI, 5.11 – 5.31), while the agonist potency, monitored as pEC_{50} of ACh, was reduced to 3.24 (95% CI, 3.16 – 3.33) (Fig. 4, E and F; Table 1). By contrast, an inverse mutation E142V in the UNC-38 subunit reduced the antagonist potency of paraherquamide A on the L-type nAChR [pIC_{50} = 7.15 (95% CI, 7.03 – 7.27)], while scarcely influencing the agonist potency of ACh (Fig. 4, G and H; Table 1).

We also tested the effects of these mutations on the agonist actions of (-)-nicotine and levamisole and on the antagonist actions of paraherquamide A in response to these ligands for both the N-type and L-type nAChRs (Fig. 5). (-)-Nicotine activated the wild-type N-type nAChR with pEC_{50} of 4.73 (95% CI, 4.64 – 4.83) (Fig. 5A; Supplemental Fig. 7A), and paraherquamide A inhibited the nicotine-induced response with pIC_{50} of 5.48 (95% CI, 5.35 – 5.61) (Supplemental Fig. 7B). However, all the mutations tested abolished the agonist action of (-)-nicotine on the N-type (ACR-16) nAChR (Fig. 5A) and did not make it an agonist of the L-type (UNC-38/UNC-29/UNC-63/LEV-1/LEV-8) nAChR (Fig. 5B).

Levamisole did not activate the wild-type or the mutant N-type nAChRs (Fig. 5C) while activating not only the wild-type but also the mutant L-type nAChRs with no significant difference in pEC_{50} (Fig. 5, D–H). However, the YDCC mutation in loop C of UNC-63 and the E142V mutation in loop E of UNC-38 reduced I_{max} (Fig. 5, E and F; Supplemental Table 1). The mutations tested hardly affected pIC_{50} of paraherquamide A on the response to levamisole (Fig. 5, G and H).

The effects of the mutations in loop C and loop E on IC_{50} values for paraherquamide A acting on the L-type (UNC-38/UNC-29/UNC-63/LEV-1/LEV-8) nAChR, albeit significant, were not as large as those observed for the corresponding mutations in the N-type (ACR-16) nAChR (Fig. 4; Table 1). Therefore, it is conceivable that other structural features may also underlie the L-type nAChR selectivity of the compound. Referring to the homology model of the N-type nAChRs in complex with paraherquamide A (Fig. 6), we postulated that Asp210 in loop C and Phe184 in loop F, both of which are only seen in the ACR-16 subunit (Fig. 3A), may contact each other, indirectly interrupting loop C–paraherquamide A interactions. No such steric interaction occurs between the proline residue in the α subunits and valine residues in the non-α subunits (UNC-29, LEV-1) in the L-type nAChR (Fig. 3A), strengthening interactions with the alkaloid. To test this hypothesis, we mutated Phe184 to valine in loop F of ACR-16 and measured the blocking potency of paraherquamide A on the mutant N-type nAChR (Fig. 7). We found that the mutation hardly affected the potency of ACh, while increasing pIC_{50} of paraherquamide A for the N-type nAChR (Fig. 7; Table 1). By contrast, both the V193F mutation in UNC-29 and the V201F mutation in LEV-1 reduced the blocking potency of paraherquamide A (Fig. 7; Table 1). On the other hand, the F184V mutation in the N-type nAChR and the V193F mutation (UNC-29) and V201F mutation (LEV-1) in the L-type nAChR had a limited impact on the agonist activity of (-)-nicotine and levamisole, respectively (Supplemental Fig. 8).

Discussion

We have investigated the antagonist actions of pararherquamide A on recombinant *C. elegans* N-type (ACR-16) and L-type (UNC-38/UNC-29/UNC-63/LEV-1/LEV-8) nAChRs expressed in *Xenopus laevis* oocytes. The L-type nAChR showed a higher paraherquamide A sensitivity compared with the N-type nAChR with a difference in pIC_{50} of 2.74 (an approximately 550-fold change in IC_{50}; Fig. 1, D and E; Table 1), consistent with findings for the *A. suum* N- and L- type nAChRs (Robertson et al., 2002). Also, the tests of the compound on the L-type 2.1 and 2.2 nAChRs (Fig. 1, J and K) and the wild-type and mutant *C. elegans* worms (Fig. 2) suggest that the higher paraherquamide sensitivity of the L-type nAChR compared with the N-type nAChR appears to hold for nAChRs of a parasitic (*A. suum*) and a free-living (*C. elegans*) nematode.

Paraherquamide A interacted competitively with ACh on the N-type nAChRs of *C. elegans* (Fig. 1F), as is the case of native *A. suum* nAChRs (Robertson et al., 2002), suggesting that the compound binds to the orthosteric site. Its noncompetitive antagonist action on the *C. elegans* L-type nAChR does not exclude interactions with the orthosteric site, because such an action can result from binding to a distinct orthosteric site from that to which ACh is bound among the orthosteric α subunit/α subunit and α subunit/non-α subunit interfaces in the L-type nAChR. Alternatively, paraherquamide A may lock the nAChR to an inactive state and prevent its activation by ACh, resulting in an apparent noncompetitive interaction as in the case of the α7 nAChR interactions with α-bungarotoxin, where the toxin allosterically inhibits the ACh-induced activation of the nAChR even though both ligands share the orthosteric site (daCosta et al., 2015).

Given the similarity to the orthosteric site of the N-type (ACR-16) nAChR in forming a homo-pentameric structure and the competitive interaction of the ACR-16 homomer with paraherquamide A, *Ls*-AChBP was used as a nAChR ligand binding domain surrogate for co-crystallization studies with the fungal alkaloid paraherquamide A. The crystal structure showed that hydrophobic interactions as well as cation-π interactions with aromatic amino acid residues appeared to play a major role in the binding of paraherquamide A to *Ls*-AChBP (Fig. 3C).

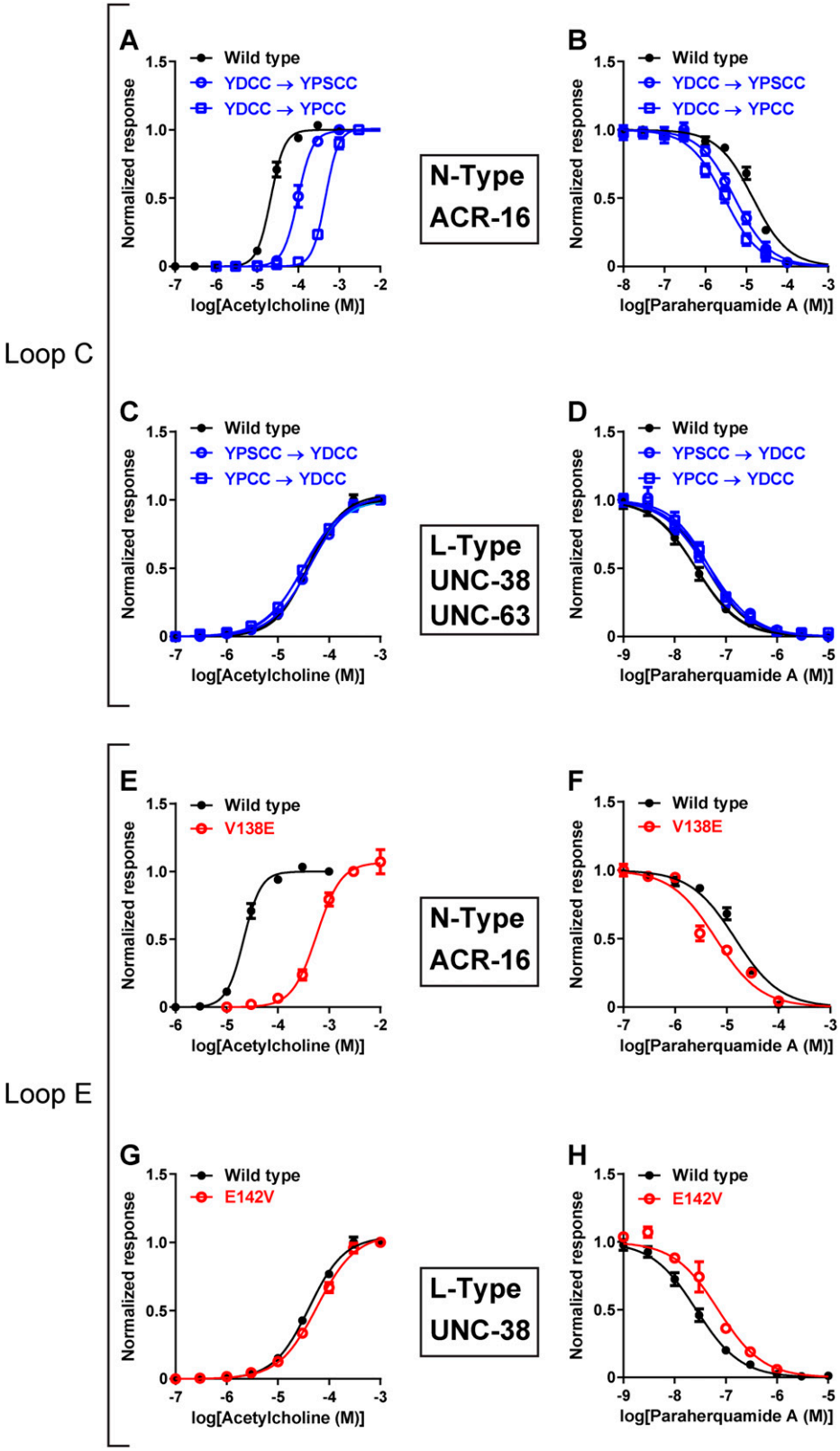

Fig. 4. Effects of mutations in loop C and loop E on agonist actions of ACh and antagonist actions of paraherquamide A on the ACh-induced response of the *C. elegans* N-type and L-type nAChRs expressed *X. laevis* oocytes. (A and B) Effects of the mutations in loop C on the actions of ACh (A) and paraherquamide A (B) on the N-type nAChR. (C and D) Effects of the mutations in loop C on the actions of ACh (C) and paraherquamide A (D) on the L-type nAChR. (E and F) Effects of the mutations in loop E on the actions of ACh (E) and paraherquamide A (F) on the N-type nAChR. (G and H) Effects of the mutations in loop E on the actions of ACh (G) and paraherquamide A (H) on the L-type nAChR. Each plotted point is mean ± S.E.M. (n = 5). Each data plot indicates the mean ± S.E.M. (n = 5). ACh concentrations: For wild-type N-type nAChRs, 10 μM; for YPSCC mutant N-type nAChR,100 μM; for V138E mutant N-type nAChR and YPCC mutant N-type nAChR, 500 μM; for wild-type and mutant L-type nAChRs, 30 μM.

However, amino acids involved in such interactions (Trp53 in loop D, Tyr89 at loop A, Trp143 in Loop B, and Tyr185 and Tyr192 in loop C) are conserved through the ACR-16, UNC-38, UNC-29, UNC-63, LEV-8, and LEV-1 subunits (Fig. 3A). Therefore, such interactions might underpin the L-type (UNC-38/UNC-29/UNC-63/LEV-1/LEV-8) nAChR selectivity only when the overall conformation of the orthosteric site is the dominant determinant of the affinity of the compound.

Paraherquamide A interacts via water with the hydroxy group of Ser186 and the main chain of Cys187 in loop C as

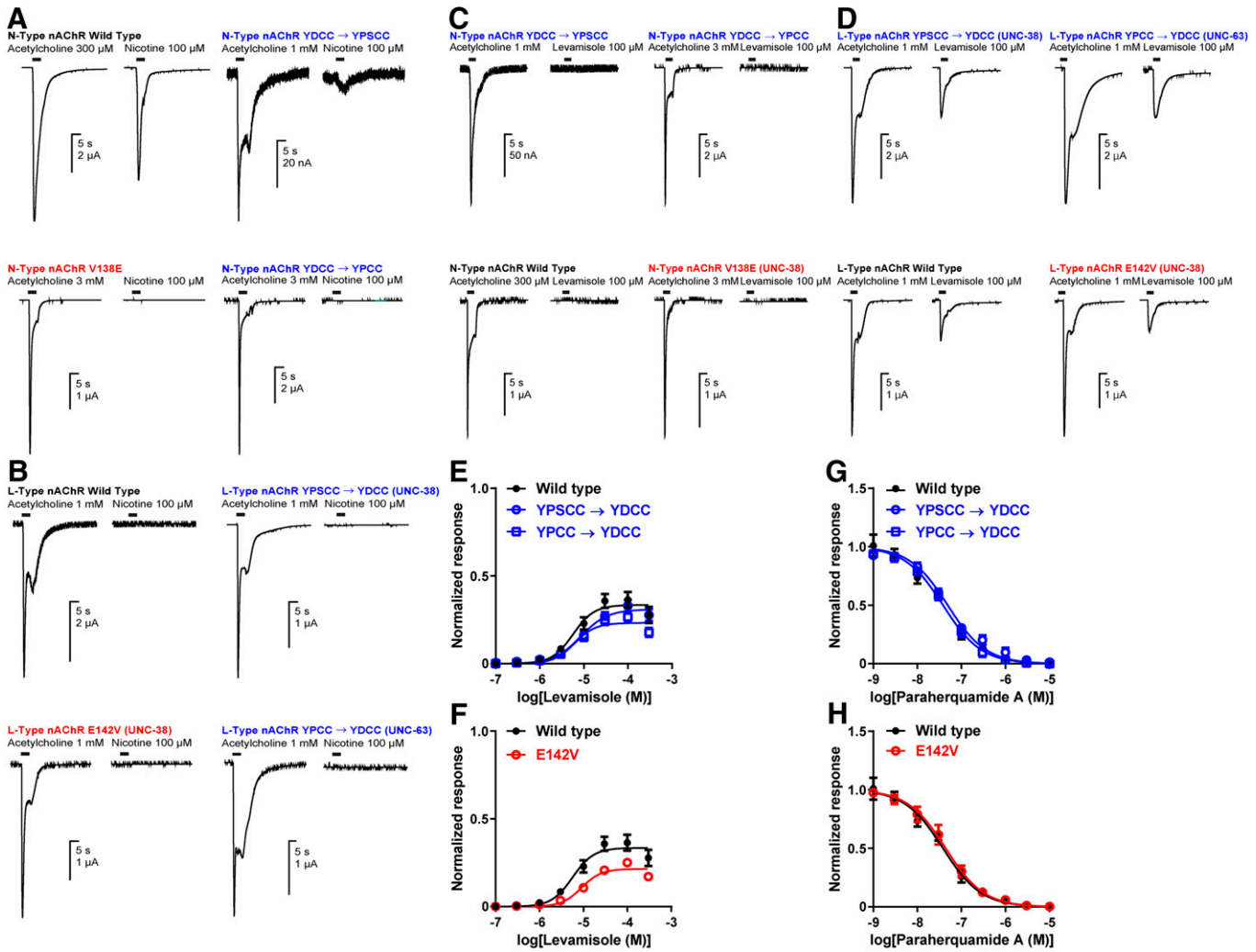

Fig. 5. Effects of mutations in loop C and loop E on the actions of (-)-nicotine and levamisole on the *C. elegans* N- and L-type nAChRs expressed *X. laevis* oocytes and antagonist actions of paraherquamide A on the levamisole induced response of the L-type nAChR. (A) Actions of (-)-nicotine on the wild type and mutant N-type nAChRs. (B) Actions of (-)-nicotine on the wild type and mutant L-type nAChRs. (C) Actions of levamisole on the on the wild-type and mutant N-type nAChRs. (D) Actions of levamisole on the wild-type and mutant L-type AChRs. (E, F) Effects of mutations in loop C (E) and loop E (F) on the agonist action of levamisole on the L-type nAChR. (G, H) Effects of mutations in loop C (G) and loop E (H) on the antagonist action of paraherquamide A for the levamisole-induced response of the L-type nAChRs. The antagonist potency of paraherquamide A was determined for the nAChR response to 10 μM levamisole. In (E), (F), (G), and (H), each plot shows the mean ± S.E.M. (n = 5).

well as the hydroxy group of Tyr164 in loop F in the crystal structure (Fig. 3, C and D). In accord with this finding, exchanging loop C between the ACR-16 (N-type nAChR) and UNC-38 (L-type nAChR) or UNC-63 subunits (L-type nAChR) led to a change of paraherquamide A potency on the N- and L-type nAChRs (Fig. 4, B and D), suggesting a contribution of the proline in loop C to determining the paraherquamide A actions. The V138E mutation in ACR-16 and E142V mutation in UNC-38 respectively enhanced and reduced the blocking potency of paraherquamide A on the N-type and L-type nAChRs (Fig. 4, F and H), demonstrating that the bridgehead nitrogen of paraherquamide A, when protonated, interacts electrostatically with the negatively charged glutamate in loop E of the UNC-38 subunit in the L-type nAChR, thereby strengthening the binding of the ligand. Derquantel was much less potent than paraherquamide A on the *C. elegans* L-type (UNC-38/UNC-29/UNC-63/LEV-1/LEV-8) nAChR (Supplemental Fig. 4) in accordance with the homology model of the *Ls*-AChBP in complex with the compound, where the lack of the carbonyl group resulted in a loss of hydrogen bonds with loop C and loop F (Supplemental Fig. 9).

The model of the N-type nAChR in complex with paraherquamide A (Fig. 6) indicated that Phe184 in loop F of ACR-16 may prevent the compound interactions with the orthosteric site by steric contacts with Asp210. Hence, we examined the effects of the F184V mutation in the ACR-16 subunit of the N-type nAChR and inverse mutations of the corresponding valines in the UNC-29 and LEV-1 subunits (V193F mutation in UNC-29 and V201F mutation in LEV-1) in the L-type nAChR on the blocking potency of paraherquamide A. We found that the F184V mutation in ACR-16 increased pIC_{50}, while the V193F mutation in UNC-29 and V201F mutation in LEV-1 decreased it (Fig. 7; Table 1), supporting our hypothesis. It is therefore conceivable that loop C, loop E, and loop F cooperatively determine the antagonist actions of the compound.

We investigated the actions of (-)-nicotine and levamisole on the wild-type and mutant N-type and L-type nAChRs (Fig. 5;

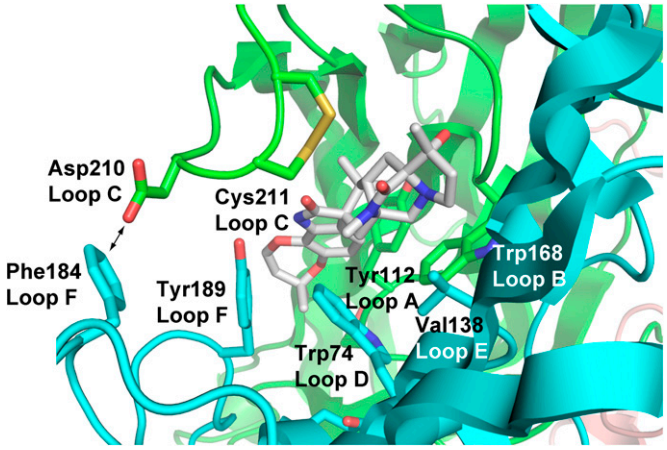

Fig. 6. Homology model of the *C. elegans* wild-type N-type nAChR in complex with paraherquamide A. The main chain in the principal and complementary side of the N-type nAChRs are colored green and cyan, respectively, while carbons, nitrogens, oxygens, and sulfurs are colored gray, blue, red, and yellow, respectively. In paraherquamide A, carbons, nitrogens, and oxygens are colored gray, blue, and red, respectively.

Supplemental Fig. 8). All the mutations in loop C and E tested abolished the agonist activity of (-)-nicotine on the N-type nAChR (Fig. 5, A and B), while the mutation in loop F had no clear impact on the agonist activity of the compound (Supplemental Fig. 8A). On the other hand, none of the mutations in loop C and loop E of the UNC-38 and UNC-63 subunits as well as of the mutations in loop F of the UNC-29 and LEV-1 enabled activation by (-)-nicotine of the L-type nAChR (Fig. 5B; Supplemental Fig. 8B). Also, all the mutations of the N-type nAChRs failed to make levamisole an agonist (Fig. 5C), and the mutations of the L-type nAChR had a limited impact on the agonist activity of levamisole and the antagonist potency paraherquamide A for the agonist action of levamisole (Fig. 5, D–H; Supplemental Fig. 8B; Table S1), suggesting differences in the modes of actions at the orthosteric site between (-)-nicotine, levamisole, and paraherquamide A.

In conclusion, we have co-crystallized the *Ls*-AChBP with paraherquamide A to elucidate determinants underpinning the L-type nAChR selectivity of the anthelmintic compound. We have shown for the first time that structural features of loop C, loop E, and loop F account for the L-type nAChR selectivity of paraherquamide A. Although other features, notably interactions either with noncompetitive site or differential interactions with α/α versus α/non-α subunit interfaces, cannot be ruled out from the mechanism of selectivity, the results offer new insights into the mode of action of paraherquamide A and a platform to assist in the design of new drugs targeting cholinergic neurotransmission of parasitic nematodes.

Acknowledgments

The authors are indebted to Steven Buckingham, School of Biological & Chemical Sciences, Queen Mary University of London, for advice on oocyte expression. The authors acknowledge Thomas Boulin for the gift of the cDNAs of *C. elegans* L-type nAChR subunits and

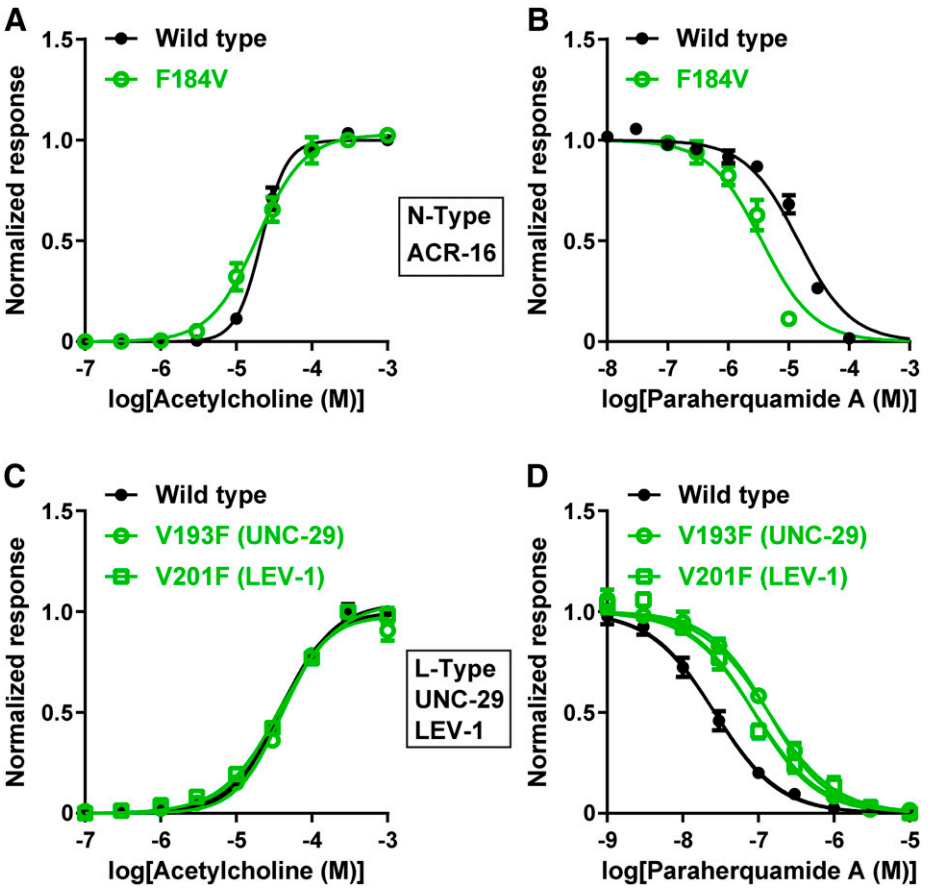

Fig. 7. Effects of mutations in loop F on agonist actions of ACh and antagonist actions of paraherquamide A on the Ach-induced responses of *C. elegans* N-type and L-type nAChRs expressed *X. laevis* oocytes. Each plotted point is mean ± S.E.M. (n = 5). (A, B) Effects of F184V mutation in loop F of the ACR-16 subunit on the actions of ACh (A) and paraherquamide A (B) on the N-type nAChR. (C, D) Effects of V193F and F201F mutations in loop F of the UNC-29 and LEV-1 subunits, respectively, on the actions of ACh (C) and paraherquamide A (D) on the L-type nAChR. Each plot represents the mean ± S.E.M. (n = 5). In B and D, antagonist actions of paraherquamide A were determined for the responses to 10 μM ACh of the N-type nAChRs and 30 μM ACh of the L-type nAChRs.

auxiliary proteins RIC-3, UNC-50, and UNC-74. The synchrotron radiation experiments were performed at the BL26B1 of SPring-8, with approvals of the Japan Synchrotron Radiation Research Institute (proposal numbers 2017A2514, 2018A2566).

Note Added in Proof: The author corrected the Imax data for (-)-Nicotine to 3 decimal places in Supplemental Table 1 in the Fast Forward version published March 22, 2023. Supplemental Table 1 has now been corrected.

Authorship Contributions

Participated in research design: Koizumi, Otsubo, Furutani, Niki, Ihara, Sattelle, Matsuda.

Conducted experiments: Koizumi, Otsubo, Furutani, Niki, Takayama, Fujimura, Maekawa, Koyari, Ihara, Kai, Hayashi, Ali, Kage-Nakadai, Matsuda.

Performed data analysis: Koizumi, Otsubo, Furutani, Niki, Koyari, Ihara, Matsuda.

Wrote or contributed to the writing of the manuscript: Koizumi, Otsubo, Furutani, Niki, Ihara, Kai, Hayashi, Kage-Nakadai, Sattelle, Matsuda.

References

Ballivet M, Alliod C, Bertrand S, and Bertrand D (1996) Nicotinic acetylcholine receptors in the nematode *Caenorhabditis elegans*. *J Mol Biol* **258:**261–269.

Bennett HM, Lees K, Harper KM, Jones AK, Sattelle DB, Wonnacott S, and Wolstenholme AJ (2012) *Xenopus laevis* RIC-3 enhances the functional expression of the *C. elegans* homomeric nicotinic receptor, ACR-16, in *Xenopus* oocytes. *J Neurochem* **123:**911–918.

Blanchard A, Guégnard F, Charvet CL, Crisford A, Courtot E, Sauvé C, Harmache A, Duguet T, O'Connor V, Castagnone-Sereno P et al. (2018) Deciphering the molecular determinants of cholinergic anthelmintic sensitivity in nematodes: when novel functional validation approaches highlight major differences between the model *Caenorhabditis elegans* and parasitic species. *PLoS Pathog* **14:**e1006996.

Blanchflower SE, Banks RM, Everett JR, Manger BR, and Reading C (1991) New paraherquamide antibiotics with anthelmintic activity. *J Antibiot (Tokyo)* **44:**492–497.

Boulin T, Gielen M, Richmond JE, Williams DC, Paoletti P, and Bessereau JL (2008) Eight genes are required for functional reconstitution of the *Caenorhabditis elegans* levamisole-sensitive acetylcholine receptor. *Proc Natl Acad Sci USA* **105:**18590–18595.

Buxton SK, Charvet CL, Neveu C, Cabaret J, Cortet J, Peineau N, Abongwa M, Courtot E, Robertson AP, and Martin RJ (2014) Investigation of acetylcholine receptor diversity in a nematode parasite leads to characterization of tribendimidine- and derquantel-sensitive nAChRs. *PLoS Pathog* **10:**e1003870.

C. elegans Sequencing Consortium (1998) Genome sequence of the nematode *C. elegans*: a platform for investigating biology. Science **282**:2012–2018.

daCosta CJ, Free CR, and Sine SM (2015) Stoichiometry for α-bungarotoxin block of α7 acetylcholine receptors. *Nat Commun* **6:**8057.

Emsley P and Cowtan K (2004) Coot: model-building tools for molecular graphics. *Acta Crystallogr D Biol Crystallogr* **60**(Pt 12 Pt 1):2126–2132.

Evans PR and Murshudov GN (2013) How good are my data and what is the resolution? *Acta Crystallogr D Biol Crystallogr* **69**:1204–1214.

Ihara M, Okajima T, Yamashita A, Oda T, Asano T, Matsui M, Sattelle DB, and Matsuda K (2014) Studies on an acetylcholine binding protein identify a basic residue in loop G on the β1 strand as a new structural determinant of neonicotinoid actions. *Mol Pharmacol* **86:**736–746.

Jones AK, Davis P, Hodgkin J, and Sattelle DB (2007) The nicotinic acetylcholine receptor gene family of the nematode *Caenorhabditis elegans*: an update on nomenclature. *Invert Neurosci* **7:**129–131.

Kabsch W (2010) Xds. *Acta Crystallogr D Biol Crystallogr* **66:**125–132.

Katoh K, Misawa K, Kuma K, and Miyata T (2002) MAFFT: a novel method for rapid multiple sequence alignment based on fast Fourier transform. *Nucleic Acids Res* **30:**3059–3066.

Katoh K and Standley DM (2013) MAFFT multiple sequence alignment software version 7: improvements in performance and usability. *Mol Biol Evol* **30:**772–780.

Lee BH, Clothier MF, Dutton FE, Nelson SJ, Johnson SS, Thompson DP, Geary TG, Whaley HD, Haber CL, Marshall VP et al. (2002) Marcfortine and paraherquamide class of anthelmintics: discovery of PNU-141962. *Curr Top Med Chem* **2:**779–793.

Matsuda K, Buckingham SD, Freeman JC, Squire MD, Baylis HA, and Sattelle DB (1998) Effects of the α subunit on imidacloprid sensitivity of recombinant nicotinic acetylcholine receptors. *Br J Pharmacol* **123:**518–524.

McCoy AJ (2007) Solving structures of protein complexes by molecular replacement with Phaser. *Acta Crystallogr D Biol Crystallogr* **63:**32–41.

Murshudov GN, Skubák P, Lebedev AA, Pannu NS, Steiner RA, Nicholls RA, Winn MD, Long F, and Vagin AA (2011) *REFMAC5* for the refinement of macromolecular crystal structures. *Acta Crystallogr D Biol Crystallogr* **67:**355–367.

Ondeyka JG, Goegelman RT, Schaeffer JM, Kelemen L, and Zitano L (1990) Novel antinematodal and antiparasitic agents from *Penicillium charlesii*. I. Fermentation, isolation and biological activity. *J Antibiot (Tokyo)* **43:**1375–1379.

Ostlind DA, Mickle WG, Ewanciw DV, Andriuli FJ, Campbell WC, Hernandez S, Mochales S, and Munguira E (1990) Efficacy of paraherquamide against immature *Trichostrongylus colubriformis* in the gerbil (*Meriones unguiculatus*). *Res Vet Sci* **48:**260–261.

Raymond V, Mongan NP, and Sattelle DB (2000) Anthelmintic actions on homomer-forming nicotinic acetylcholine receptor subunits: chicken α7 and ACR-16 from the nematode *Caenorhabditis elegans*. *Neuroscience* **101:**785–791.

Robertson AP, Bjorn HE, and Martin RJ (1999) Resistance to levamisole resolved at the single-channel level. *FASEB J* **13:**749–760.

Robertson AP, Clark CL, Burns TA, Thompson DP, Geary TG, Trailovic SM, and Martin RJ (2002) Paraherquamide and 2-deoxy-paraherquamide distinguish cholinergic receptor subtypes in Ascaris muscle. *J Pharmacol Exp Ther* **302:**853–860.

Schaeffer JM, Blizzard TA, Ondeyka J, Goegelman R, Sinclair PJ, and Mrozik H (1992) [^{3}H]paraherquamide binding to *Caenorhabditis elegans*. Studies on a potent new anthelmintic agent. *Biochem Pharmacol* **43:**679–684.

Thompson DP, Klein RD, and Geary TG (1996) Prospects for rational approaches to anthelmintic discovery. *Parasitology* **113**(Suppl):S217–S238.

Trott O and Olson AJ (2010) AutoDock Vina: improving the speed and accuracy of docking with a new scoring function, efficient optimization, and multithreading. *J Comput Chem* **31:**455–461.

Wallace AC, Laskowski RA, and Thornton JM (1995) LIGPLOT: a program to generate schematic diagrams of protein-ligand interactions. *Protein Eng* **8:**127–134.

Webb B and Sali A (2016) Comparative protein structure modeling using MODELLER. *Curr Protoc Bioinformatics* **54**:5.6.1–37.

Winn MD, Ballard CC, Cowtan KD, Dodson EJ, Emsley P, Evans PR, Keegan RM, Krissinel EB, Leslie AG, McCoy A et al. (2011) Overview of the CCP4 suite and current developments. *Acta Crystallogr D Biol Crystallogr* **67:**235–242.

Yamazaki M, Okuyama E, Kobayashi M, and Inoue H (1981) The structure of paraherquamide, a toxic metabolite from *Penicillium paraherquei*. *Tetrahedron Lett* **22:**135–136.

Zinser EW, Wolf ML, Alexander-Bowman SJ, Thomas EM, Davis JP, Groppi VE, Lee BH, Thompson DP, and Geary TG (2002) Anthelmintic paraherquamides are cholinergic antagonists in gastrointestinal nematodes and mammals. *J Vet Pharmacol Ther* **25:**241–250.

Address correspondence to: Kazuhiko Matsuda, Department of Applied Biological Chemistry, Faculty of Agriculture, Kindai University, 3327-204 Nakamachi, Nara 631-8505, Japan. E-mail: kmatsuda@nara.kindai.ac.jp